GEOLOGICA CARPATHICA, 2026, 77, 4, 275–289 https://doi.org/10.31577/GeolCarp.2026.14

Cr-spinel compositions and the petrogenesis of podiform chromitites in the Kağızman Ophiolite (Ağrı, Eastern Türkiye)

LEVENT ASLAN[1] and TIJEN ÜNER[2,✉]

[1]Van Yüzüncü Yıl University, Institute of Natural and Applied Sciences, Van, Türkiye
[2]Van Yüzüncü Yıl University, Department of Geological Engineering, Van, Türkiye

(Manuscript received January 19, 2026; accepted in revised form May 26, 2026; Associate Editor: Igor Broska)

Abstract: Podiform chromitites are important indicators of mantle processes associated with subduction initiation, yet their formation mechanisms remain debated. This study presents petrographic and mineral-chemical data from chromitites of the Eastern Ağrı region (Kağızman Ophiolite) in the eastern segment of the İzmir–Ankara–Erzincan Suture Zone and evaluates their significance for supra-subduction zone (SSZ) forearc mantle evolution along the northern Neo-Tethyan margin. The chromitites occur as massive and disseminated bodies hosted by dunite channels within refractory harzburgite. Sharp spinel grain boundaries and primary silicate inclusions (orthopyroxene±olivine) preserved within Cr-spinel cores indicate focused melt flow, melt–rock interaction, and chromitite saturation in a forearc mantle setting. Cr-spinels are characterized by high Cr# values (0.57–0.88) and low TiO_2 contents (<0.7 wt.%), whereas olivine ($Fo_{90–93}$) and orthopyroxene (Mg#=90–94) compositions indicate a strongly depleted mantle source. Field relationships, petrography, and mineral chemistry suggest that chromitite formation occurred during subduction initiation and was related to slab-derived fluid influx and hydrous melting of refractory mantle. The coexistence of different chromitite textures and preserved primary mineral signatures indicates a multi-stage chromitite-forming process linked to evolving melt fluxes. Comparison with other Neo-Tethyan and global ophiolitic chromitites supports an SSZ affinity for the Kağızman chromitites and highlights the role of integrated petrographic and mineral-chemical approaches in constraining chromitite genesis and forearc mantle evolution.

Keywords: Cr-spinel chemistry, forearc mantle, melt–rock interaction, Neo-Tethyan ophiolites, supra-subduction zone (SSZ)

Introduction

Eastern Anatolia occupies a critical position within the Alpine–Himalayan orogenic belt, where remnants of the Neo-Tethyan oceanic lithosphere preserve an unusually complete record of subduction initiation, forearc magmatism, and ophiolite emplacement. The region represents one of the few segments of the Neo-Tethyan realm in which mantle-derived lithologies, arc-related magmatic products, and suture-zone structures are spatially and temporally well preserved, providing a unique natural laboratory for investigating early subduction processes and forearc mantle evolution (Okay & Tüysüz 1999; Dilek & Furnes 2011; Moghadam et al. 2020).

Prior to Neo-Tethyan ocean opening, Eastern Anatolia formed part of the northern passive margin of Gondwana, represented by metamorphic basement complexes and overlying sedimentary successions. This configuration was profoundly modified during the Mesozoic by the opening and subsequent closure of the Neo-Tethys Ocean, particularly its northern branch, the İzmir–Ankara–Erzincan Ocean (IAEO). Late Cretaceous subduction of the IAEO beneath the Eurasian margin resulted in widespread supra-subduction zone (SSZ) magmatism, large-scale ophiolite emplacement, and the development of the İzmir–Ankara–Erzincan Suture Zone (IAESZ), one of the most prominent tectonic boundaries in Anatolia (Şengör & Yılmaz 1981; Stampfli & Borel 2002; Robertson et al. 2014). Subsequent Arabia–Eurasia collision during the Cenozoic further reworked these ophiolitic fragments, yet significant portions of the mantle sections remain remarkably well preserved (Okay & Şengör 1992; Şaroğlu et al. 1992; Rolland 2017).

The İzmir–Ankara–Erzincan Suture Zone (IAESZ) hosts a series of discontinuous ophiolitic bodies extending from western to eastern Anatolia and represents the principal remnant of the northern branch of the Neo-Tethys. These ophiolites display pronounced along-strike variations in mantle lithology, magmatic affinity, and degree of depletion, reflecting spatial heterogeneity in subduction initiation processes along the Neo-Tethyan margin (Dilek & Furnes 2011; Robertson et al. 2014; Moghadam et al. 2020). Western and central IAESZ ophiolites are commonly characterized by refractory harzburgitic mantle sections, well-developed SSZ geochemical signatures, and widespread podiform chromitites, whereas eastern segments tend to preserve more fragmented

✉ corresponding author: Tijen Üner
tcakici@yyu.edu.tr

and tectonically reworked mantle assemblages affected by later collisional deformation. This eastward variability highlights the importance of region-specific studies for evaluating whether chromitite-forming processes were uniform along the IAESZ or varied in response to local mantle dynamics, melt fluxes, and evolving slab–mantle interactions during subduction initiation.

Within this tectonic framework, Eastern Anatolia ophiolites are widely interpreted as fragments of Late Cretaceous SSZ oceanic lithosphere generated during subduction initiation (Dilek & Furnes 2011; van Hinsbergen et al. 2020). Their lithological architecture – dominated by refractory harzburgites and dunites, locally intruded by gabbroic bodies and sheeted dykes and overlain by arc-related volcanic and pelagic sedimentary units – together with HFSE-depleted and LILE-enriched geochemical signatures, is characteristic of forearc mantle environments (Pearce et al. 1984; Shervais & Jean 2012; Pearce 2014). Such conditions are increasingly recognized as optimal for the formation of podiform chromitites through focused melt–rock interaction between highly depleted mantle peridotites and high-Mg hydrous melts during subduction initiation (Arai & Miura 2016; Farré-de-Pablo et al. 2020).

Podiform chromitites constitute some of the most sensitive petrological archives of mantle processes in SSZ settings. Variations in Cr-spinel chemistry – particularly Cr#, Mg#, and Fe^{3+} contents – together with the compositions of coexisting olivine and orthopyroxene, provide robust constraints on the degree of mantle depletion, the nature of parental melts (boninitic versus arc-tholeiitic), and the intensity of melt–rock interaction during chromitite formation (Kamenetsky et al. 2001; Rollinson 2008; Arai 2013). Recent high-resolution studies further demonstrate that many SSZ chromitites record multi-stage melt infiltration and re-equilibration while preserving primary magmatic signatures despite later serpentinization, provided that mineral-chemical criteria are carefully evaluated (Miura et al. 2012; Fornasaro et al. 2023; Liu et al. 2023).

Across Türkiye and the eastern Mediterranean, chromitites hosted by Neo-Tethyan ophiolites are increasingly interpreted as key indicators of subduction initiation and early forearc mantle evolution. Integrated mineral-chemical, isotopic, and PGE-based studies from the Köyceğiz, Kızıldağ, Kırdağ, and Mersin ophiolites document high-Cr chromitites formed through interaction between highly depleted mantle peridotite and boninitic to arc-tholeiitic melts, locally accompanied by isotopic evidence for slab-derived and deep mantle contributions (Uysal et al. 2014; Xiong et al. 2022; Bilici 2025). However, despite its strategic position along the eastern segment of the IAESZ, the Kağızman Ophiolite has remained largely unexplored within this mineral-chemical framework.

As a result, it remains unclear whether chromitite formation in the Kağızman region records subduction-initiation processes comparable to those documented farther west along the Neo-Tethyan forearc, or whether it reflects distinct melt–rock interaction pathways related to spatial heterogeneity in the eastern forearc mantle. This study addresses this gap by presenting the first integrated petrographic and mineral-chemical dataset for podiform chromitites from the Kağızman Ophiolite (northern Ağrı Province). By combining detailed Cr-spinel, olivine, and orthopyroxene compositions with textural constraints, we evaluate competing genetic models for chromitite formation in SSZ environments and constrain mantle depletion trends, parental melt characteristics, and melt–rock interaction processes. The results provide new insights into the spatial variability of subduction-initiation magmatism along the eastern Neo-Tethyan forearc and demonstrate the effectiveness of chromitite mineral chemistry as a high-fidelity recorder of early subduction dynamics, even in tectonically complex orogenic belts.

Geological setting

The Kağızman Ophiolite is situated in the easternmost segment of the İzmir–Ankara–Erzincan Suture Zone (IAESZ), which represents the northern closure of the Neo-Tethys Ocean in Anatolia (Şengör & Yılmaz 1981; Okay & Tüysüz 1999) (Fig. 1a). The IAESZ records Late Cretaceous northward subduction of the İzmir–Ankara–Erzincan Ocean beneath the Eurasian margin, followed by ophiolite emplacement during subduction initiation and early convergence (Stampfli & Borel 2002; Dilek & Furnes 2011). This tectonic framework was subsequently overprinted by Cenozoic Arabia–Eurasia collision, resulting in deformation, uplift, and partial dismemberment of ophiolitic units throughout Eastern Anatolia (Şaroğlu et al. 1992; Rolland 2017).

The Kağızman Ophiolite crops out north of Ağrı Province between the villages of Dumanlı, Mollaali, and Akdana, where it is exposed as tectonically dismembered ultramafic–mafic slices thrust over Eocene–Miocene sedimentary successions, including sandstones and limestones (Fig. 2a, c). Field relationships indicate that the ophiolitic units form isolated and discontinuous bodies rather than a coherent stratigraphic sequence, reflecting strong tectonic disruption during emplacement and subsequent deformation.

The mantle section is dominated by variably serpentinized harzburgite, which constitutes the main lithology exposed in the study area (Fig. 2b). The harzburgites are typically fractured and brecciated, displaying pervasive serpentinization along fracture networks and grain boundaries. Dunite occurs as irregular lenses and bands within the harzburgite and commonly hosts podiform chromitite bodies. Chromitites are observed both as massive lenses and as disseminated aggregates of chromian spinel within dunite envelopes, with sharp contacts against the surrounding harzburgite (Fig. 2d). Individual chromitite bodies range from decimetre- to metre-scale and exhibit lenticular to irregular geometries consistent with tectonically modified mantle-hosted chromitites.

Mafic lithologies are scarce within the Kağızman Ophiolite and are represented by isolated gabbroic bodies and diabase dykes that locally crosscut the mantle peridotites. These dykes

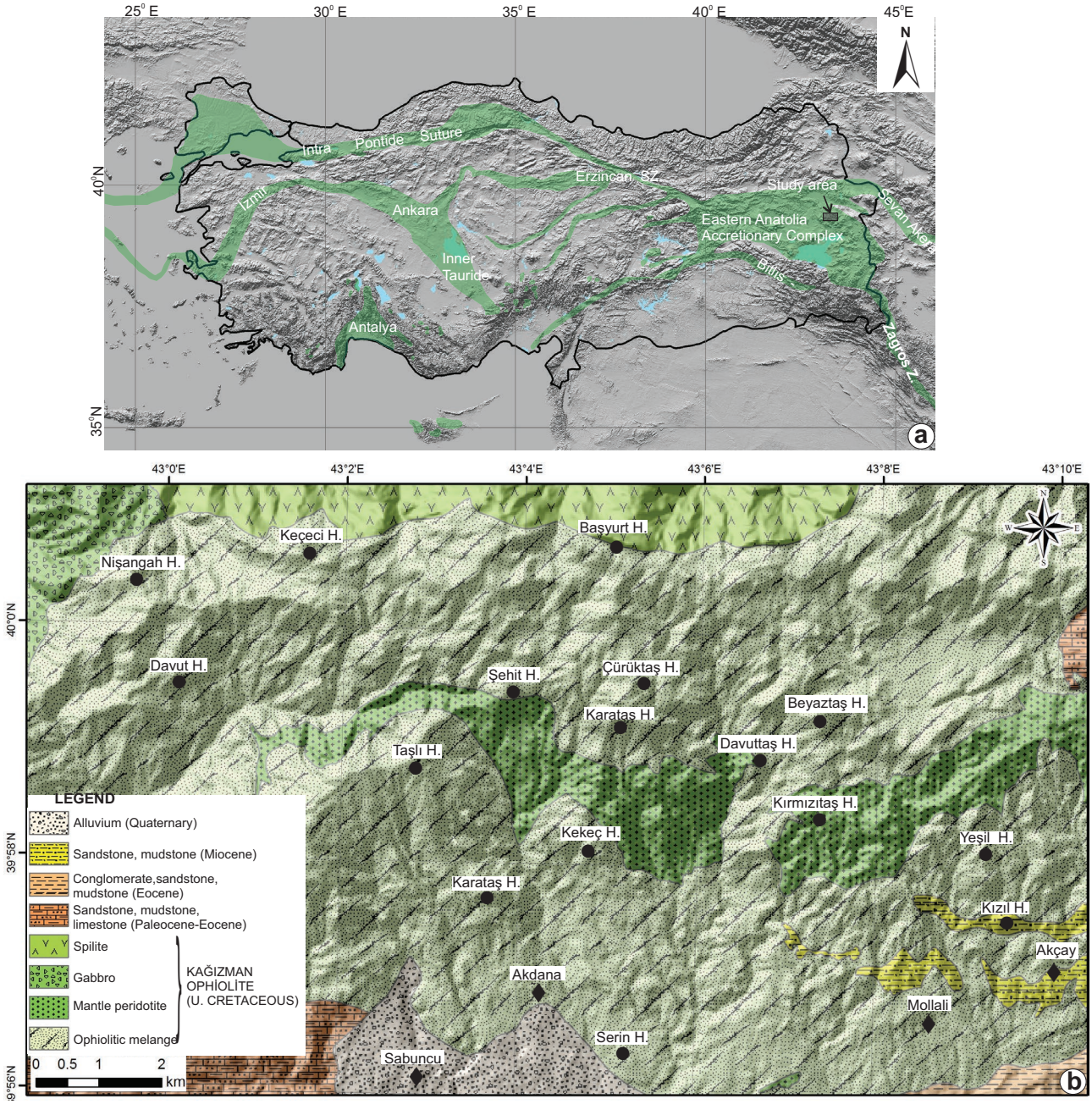

Fig. 1. Geological location of the Kağızman Ophiolite: **(a)** Simplified tectonic map of Türkiye showing the position of the İzmir–Ankara–Erzincan Suture Zone and the study area (modified after Knipper et al. 1986). **(b)** Simplified geological map of the Kağızman region showing the distribution of ophiolitic units and chromitite occurrences (modified after Sümengen 2009).

are generally narrow and discontinuous, indicating late-stage mafic magmatism within the mantle section. No complete crustal sequence is preserved, and volcanic units are absent in the immediate study area.

Serpentinization is pervasive throughout the mantle rocks and locally accompanied by late-stage vein networks composed of serpentine±carbonate minerals. Despite this alteration, chromitite bodies commonly preserve sharp field contacts with their host dunites and harzburgites, and chromian spinel grains lack visible ferritchromitite rims at the outcrop scale.

These field relationships indicate that primary textural features of the chromitites are locally well preserved, providing a suitable basis for petrographic and mineral-chemical investigation. Within this geological framework, detailed petrographic analysis is essential for documenting the microstructural characteristics of chromitites, associated dunites, and host harzburgites, and for evaluating the extent to which primary magmatic features have been preserved at the microscopic scale.

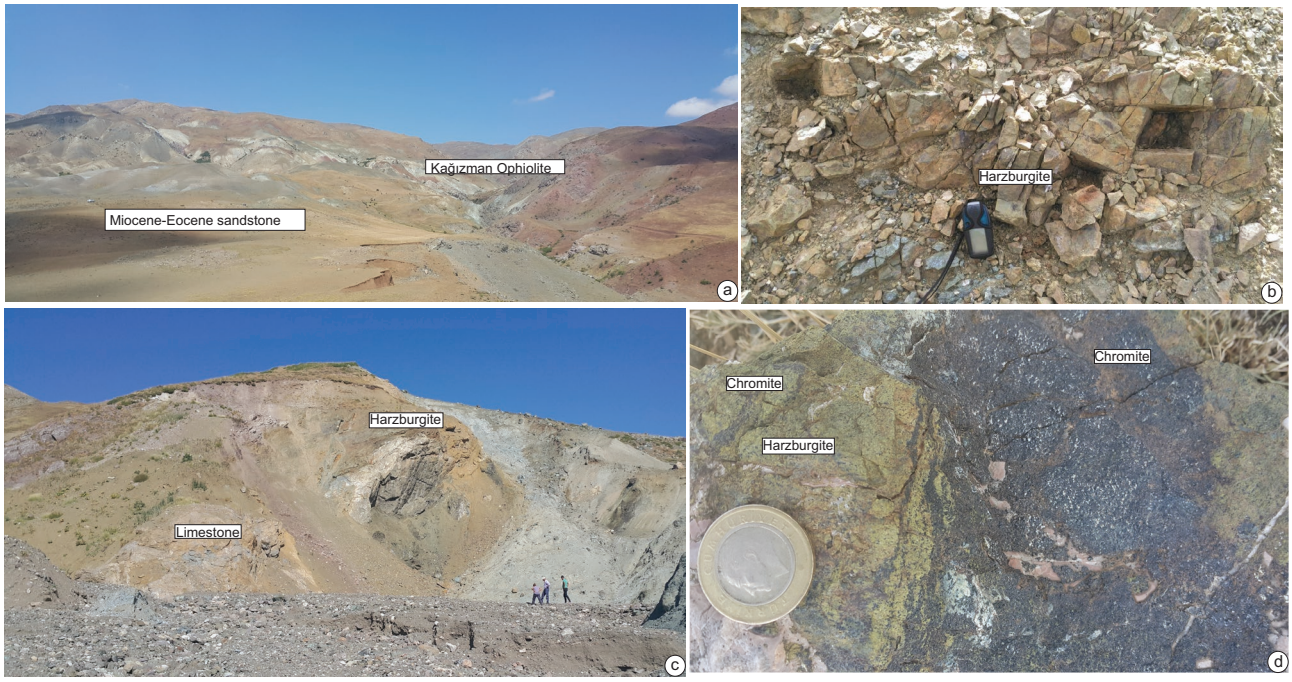

Fig. 2. Field photographs illustrating the occurrence of chromitites in the northern part of the Ağrı region (Kağızman Ophiolite): **(a)** Tectonic emplacement of Kağızman ophiolitic units over Miocene-aged sedimentary cover units; **(b)** Limestone blocks and lenses frequently enclosed within the ultramafic rocks; **(c)** Strongly serpentinized peridotite forming the dominant lithology of the mantle section; **(d)** Disseminated to layered chromitite mineralization hosted by peridotite.

Material and methods

Sampling and petrography

A total of 22 representative samples were collected from massive and disseminated podiform chromitite bodies, their surrounding dunite envelopes, and the harzburgitic host rocks within the Kağızman Ophiolite. Sampling focused on fresh, unweathered outcrops to minimize alteration effects. Chromitite lenses were sampled along strike and dip to capture internal variability, and particular attention was given to collecting samples from the harzburgitic host rocks in order to constrain melt–rock interaction processes. All samples were examined petrographically using standard optical microscopy.

Sample information, including coordinates, lithology, petrographic characteristics, and analytical usage, is summarized in Table 1.

Selection of samples for mineral chemistry

Based on petrographic characteristics, textural preservation, and representativeness of the chromitite–dunite–harzburgite association, two samples were selected for detailed mineral chemical analyses. These samples were chosen to best represent the compositional features of the chromitite bodies and their host peridotites, and to minimize the effects of alteration.

Electron microprobe analysis

Mineral chemical compositions of Cr-spinels, olivine, and orthopyroxene were analyzed using a JEOL JXA-8230 electron microprobe at the Ankara University Central Research Laboratory (YEBİM). Analytical conditions included an accelerating voltage of 15 kV and a beam current of 20 nA. A focused beam was used for spinel analyses, whereas a defocused beam with a diameter of 5 µm was applied for silicate minerals to minimize alkali loss.

Standards consisted of well-characterized synthetic oxides and natural minerals. Matrix corrections were performed using the CITZAF algorithm. Analytical conditions, including counting times and detection limits, were optimized to ensure high analytical precision and accuracy.

A total of 99 Cr-spinel, 41 olivine, and 34 orthopyroxene point analyses were performed on the selected samples to ensure representative mineral-chemical characterization.

Data processing and parameters

Compositional parameters such as Cr# [Cr/(Cr+Al)], Mg# [Mg/(Mg+Fe^{2+})], and Fe^{3+}# were calculated following established formulations (Arai 1994; Kamenetsky et al. 2001). Olivine (Fo content, NiO) and orthopyroxene (Mg#, Al_2O_3, Cr_2O_3, TiO_2) compositions were evaluated to constrain mantle depletion and melt–rock interaction processes, following approaches outlined in Sobolev et al. (2005) and Herzberg et al. (2014).

Results

Petrography

The host rocks of the Kağızman chromitites are dominantly serpentinized harzburgites that locally grade into dunite. Although serpentinization is pervasive, primary mantle textures and mineralogical relationships are commonly preserved, allowing detailed petrographic characterization. At the microscale, SEM–EDS elemental mapping reveals a heterogeneous distribution of Cr-spinel aggregates and Mg-rich silicate phases within the serpentinized peridotites (Fig. 3a), reflecting primary magmatic segregation of chromitite and subsequent hydration of the mantle host.

In thin section, massive chromitites are dominated by coarse, subhedral to euhedral Cr-spinel grains with sharp crystal boundaries, commonly crosscut by fractures filled with secondary serpentine±carbonate (Fig. 3b). Despite pervasive fracturing, Cr-spinel grains generally lack thick alteration rims at the optical scale, indicating preservation of primary magmatic compositions.

Disseminated to nodular chromitite textures are characterized by subhedral to anhedral Cr-spinel grains irregularly distributed within a serpentinized olivine-rich matrix (Fig. 3c). Spinel–silicate boundaries are typically sharp, and spinel grains locally form patchy to mosaic-like aggregates, a texture widely regarded as diagnostic of podiform chromitites formed by focused melt–rock interaction in supra-subduction zone mantle settings.

Orthopyroxene occurs mainly as coarse porphyroclasts embedded in the serpentinized matrix and commonly displays internal deformation features such as undulose extinction, lattice bending, and microfracturing (Fig. 3d). Microfractures within orthopyroxene are locally filled by secondary serpentine, indicating that fluid-assisted alteration postdated the development of primary deformation fabrics.

Relict orthopyroxene grains are also observed under cross-polarized light, where they are embedded in a fine-grained serpentinized matrix and preserve primary optical properties despite extensive hydration (Fig. 3e). Olivine is largely serpentinized but locally preserved as relict grains with high birefringence and irregular grain boundaries, reflecting progressive replacement during hydration of the mantle wedge.

In several samples, Cr-spinel mineralization is associated with chromitite-bearing dunite, where spinel grains are intergrown with serpentinized olivine (Fig. 3f). Such textures reflect focused melt flow and melt–rock interaction within dunitic channels and are consistent with chromitite saturation from high-Mg melts migrating through a depleted mantle section.

Overall, the petrographic characteristics of the Kağızman chromitites and their host peridotites-including preserved mantle deformation fabrics, dunite-associated chromitite mineralization, sharp Cr-spinel–silicate boundaries, and limited post-magmatic alteration of spinel-are typical of podiform chromitites formed in supra-subduction zone mantle environments.

Table 1: Summary of sampled lithologies, petrographic characteristics, and analytical usage from the Kağızman Ophiolite. Coordinates are given in the UTM projection (Zone 38S, WGS84 datum). The positional accuracy of the GPS measurements is estimated to be ±7 m. All samples were examined petrographically, whereas detailed mineral chemical analyses were performed only on selected representative samples.

Sample ID	Easting	Northing	Host Rock	Petrography	Microprobe Analysis
Z_6	338480	4421883	Harzburgite	ol+opx+chromitite	⊗
Z_9	338488	4421890	Harzburgite	ol+opx+chromitite	⊗
Z_10	338503	4421930	Harzburgite	ol+opx+chromitite	⊗
Z_15	338508	4421934	Harzburgite	ol+opx+chromitite	⊗
Z_18	338523	4421930	Harzburgite	ol+opx+chromitite	⊗
Z_23	338523	4421930	Harzburgite	ol+opx+chromitite	⊗
ST_4	338515	4421940	Harzburgite	ol+opx+chromitite	⊗
ST_4X	**338515**	**4421940**	**Harzburgite**	**ol+opx+chromitite**	✓
ST_9	338487	4421927	Harzburgite	ol+opx+chromitite	⊗
ST_10X	338469	4421868	Harzburgite	ol+opx+chromitite	⊗
ST_25	338580	4421943	Harzburgite	ol+opx+chromitite	⊗
CR_4	340594	4423667	Chromitite	chromitite	⊗
CR_5	340626	4423759	Chromitite	chromitite	⊗
CR_7	340635	4423810	Chromitite	chromitite	⊗
CR_8	340577	4423798	Chromitite	chromitite	⊗
LB_2	340584	4423734	Harzburgite	ol+opx+chromitite	⊗
LB_4	**340624**	**4423816**	**Harzburgite**	**ol+opx+chromitite**	✓
LB_5	340582	4423750	Harzburgite	ol+opx+chromitite	⊗
ZYD_1	340608	4423879	Dunite	ol+chromitite	⊗
ZYD_3	340592	4423876	Dunite	ol+chromitite	⊗
ZYD_4	340612	4423866	Dunite	ol+chromitite	⊗
ZYD_8	340574	4423846	Dunite	ol+chromitite	⊗

Mineral chemistry

Cr-spinels from chromitites and associated peridotites of the Kağızman Ophiolite exhibit a wide compositional spectrum. Major-element compositions (Table 2, Supplementary Table S1) show Cr_2O_3 contents ranging from 42.31 to 65.21 wt.% and Al_2O_3 contents from 6.05 to 23.15 wt.%. NiO concentrations (0.19–0.65 wt.%) fall within the typical range of mantle-derived chromitites, whereas FeO and TiO_2 contents vary between 14.45–19.68 wt.% and 0.20–0.64 wt.%, respectively. Cr# values range from 0.57 to 0.88, indicating significant compositional variability within the dataset.

The Cr-spinel compositions plotted in the Cr#–Mg# classification diagram (Fig. 4a) are predominantly distributed within the magnesiochromitite field, with a limited number of analyses extending toward the chromitite field. The inverse relationship between Cr# and Mg# values (Fig. 4b) defines a systematic compositional trend characteristic of depleted mantle-derived chromitites. In addition, low Fe^{3+} contents (0.002–0.092 apfu), low Fe_2O_3 contents (<8 wt.%), and

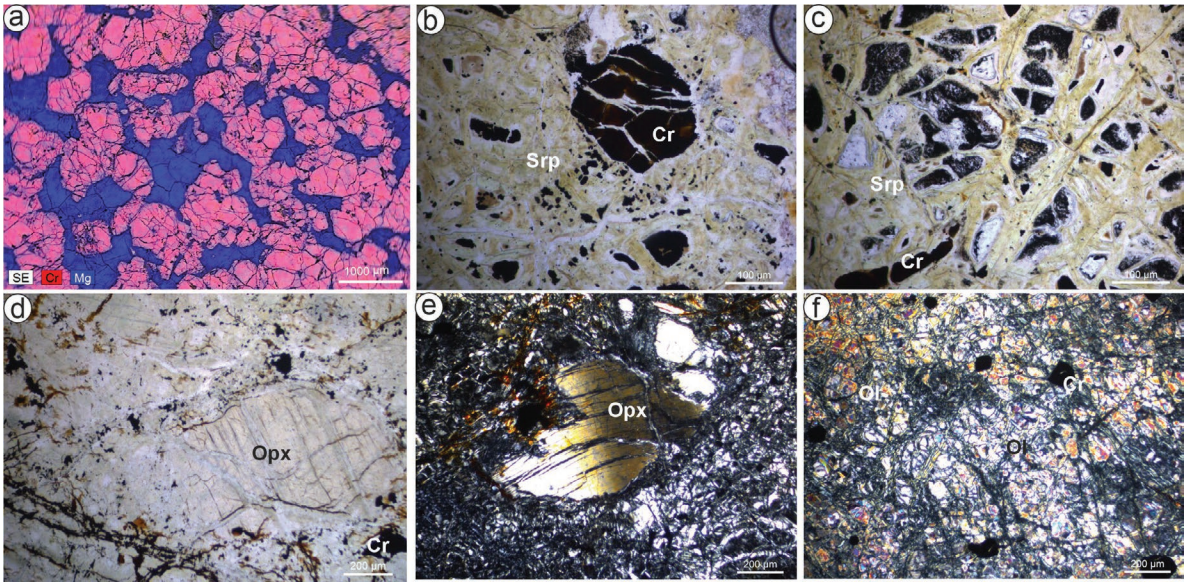

Fig. 3. Petrographic and microtextural characteristics of the Kağızman chromitites and their host peridotites: **(a)** SEM–EDS elemental map showing the distribution of Cr (red) and Mg (blue) within a serpentinized peridotite, highlighting the spatial relationship between Cr-spinel aggregates and Mg-rich silicate phases. **(b)** Plane-polarized light (PPL) image of massive chromitite composed of coarse, subhedral to euhedral Cr-spinel grains surrounded by a serpentinized matrix. **(c)** PPL image of disseminated to nodular chromitite texture characterized by irregularly distributed Cr-spinel grains within a serpentinized olivine-rich matrix. **(d)** PPL image of an orthopyroxene porphyroclast showing internal deformation features, including microfracturing, with fractures locally filled by secondary serpentine. **(e)** Cross-polarized light (XPL) image of a relict orthopyroxene grain embedded in a fine-grained serpentinized matrix, illustrating preservation of primary mantle silicates despite extensive hydration. **(f)** XPL image of chromitite-bearing dunite, showing Cr-spinel grains intergrown with serpentinized olivine, reflecting focused melt flow and melt–rock interaction within dunitic channels.

Table 2: Representative electron microprobe analyses, structural formulae, compositional parameters, and end-member proportions of Cr-spinels from the Kağızman ophiolite chromitites. Structural formulae were calculated on the basis of 32 oxygens. Abbreviations: Chr=chromitite; MgChr=magnesiochromitite; Hc=hercynite; Spl=spinel; Mt=magnetite.

Sample ID	ST 4X_10	ST 4X_26	ST 4X_44	LB 4_29	LB 4_32	LB 4_38
Cr_2O_3	50.53	59.86	42.31	65.21	44.35	52.95
Al_2O_3	17.03	10.48	23.15	6.05	22.20	17.44
TiO_2	0.26	0.28	0.55	0.39	0.24	0.37
FeO	18.62	18.69	15.77	18.52	18.14	15.77
MgO	13.03	10.09	17.54	9.43	14.35	13.05
MnO	0.32	0.41	0.28	0.45	0.42	0.31
NiO	0.54	0.33	0.51	0.48	0.47	0.49
Total	100.33	100.14	100.11	100.53	100.17	100.37
Cr	1.249	1.557	0.992	1.732	1.066	1.308
Al	0.628	0.406	0.809	0.240	0.795	0.642
Ti	0.006	0.007	0.012	0.010	0.005	0.009
Fe^{3+}	0.110	0.023	0.174	0.009	0.128	0.032
Fe^{2+}	0.377	0.492	0.217	0.512	0.333	0.380
Mg	0.607	0.495	0.776	0.472	0.650	0.608
Mn	0.008	0.011	0.007	0.013	0.011	0.008
Ni	0.014	0.009	0.012	0.013	0.011	0.012
Total	3.000	3.000	3.000	3.000	3.000	3.000
Mg#	0.62	0.50	0.78	0.48	0.66	0.62
Cr#	0.67	0.79	0.55	0.88	0.57	0.67
Fe^{3+}#	0.06	0.01	0.09	0.00	0.06	0.02
Fe^{2+}#	0.38	0.50	0.22	0.52	0.34	0.38
Al#	0.32	0.20	0.41	0.12	0.40	0.32
Chr (mol%)	24.91	39.30	11.81	45.58	18.95	25.63
MgChr	40.18	39.56	42.13	42.07	37.02	41.01
Hc (mol%)	12.52	10.25	9.63	6.30	14.14	12.59
Spl (mol%)	20.19	10.32	34.36	5.82	27.62	20.14
Mt (mol%)	2.20	0.57	2.07	0.23	2.28	0.63
Species	MgChr	MgChr	MgChr	Chr	MgChr	MgChr

relatively high MgO contents (>15 wt.%) indicate limited post-magmatic alteration and the preservation of primary magmatic signatures.

Cr-spinel compositions define a well-developed mantle array in Cr_2O_3–Al_2O_3 space (Fig. 5a), characterized by decreasing Al_2O_3 with increasing Cr_2O_3. This trend reflects systematic compositional variation across the dataset. In the TiO_2–Al_2O_3 diagram (Fig. 5b), most analyses cluster at low TiO_2 values and moderate Al_2O_3 contents, forming a coherent array distinct from typical MORB fields. Additional constraints are provided by Mn systematics (Fig. 5c), where the majority of data plot within the primary Cr-spinel field, with limited dispersion toward higher MnO values. The Cr#–Mg# diagram (Fig. 5d) shows a negative correlation, with samples forming a continuous trend toward higher Cr# at lower Mg# values.

Trace-element and divalent cation relationships further illustrate systematic compositional behavior of Cr-spinels (Fig. 6a–d). A strong negative correlation

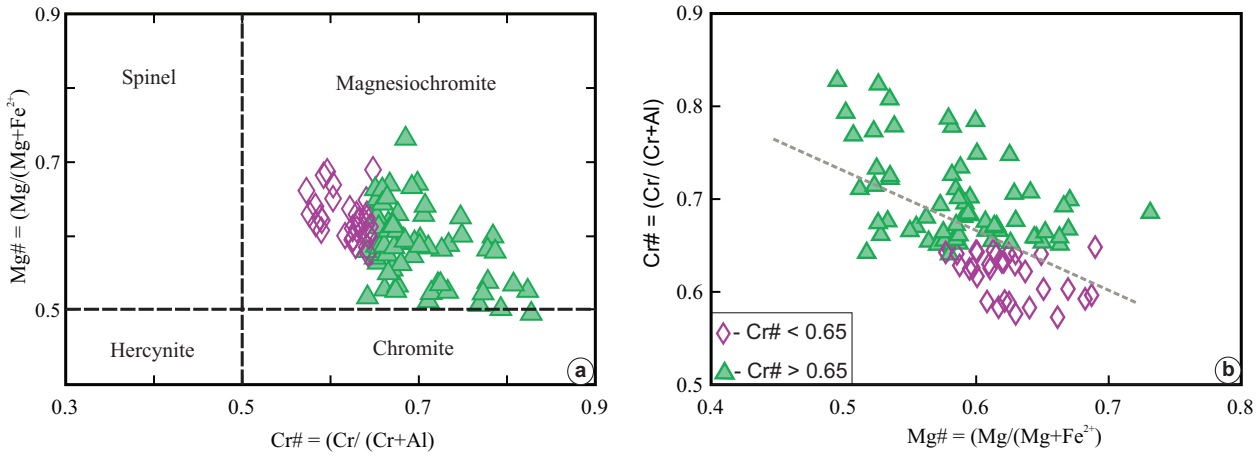

Fig. 4. (a) Classification diagram of analyzed Cr-spinels based on Cr# and Mg# values showing chromitite and magnesiochromitite compositional fields (modified after Kapsiotis 2013; Aslan et al. 2025). **(b)** Relationship between Cr# and Mg# values of analyzed Cr-spinels.

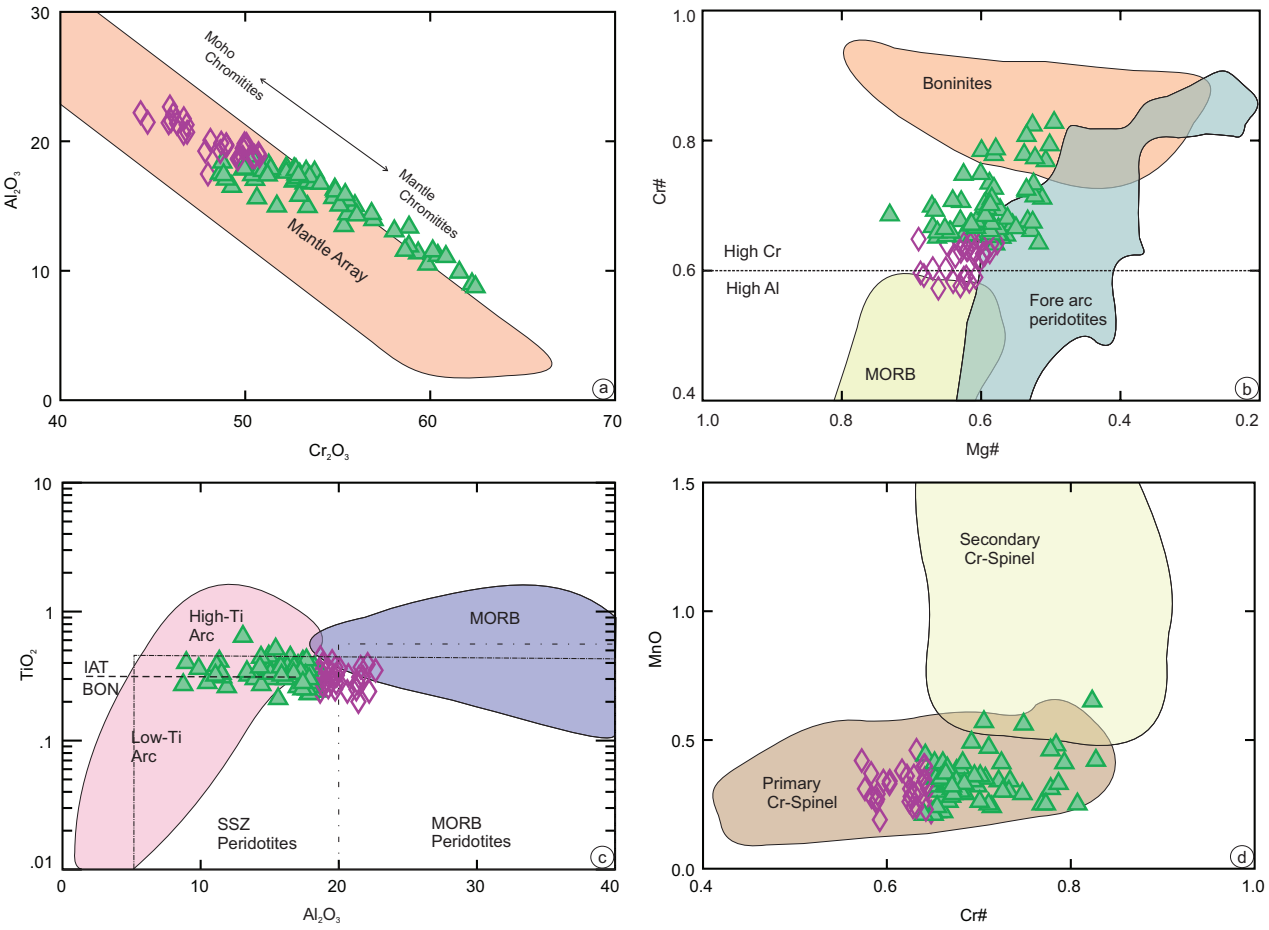

Fig. 5. Cr-spinel compositions from the Kağızman chromitites plotted on selected discrimination diagrams: **(a)** Cr_2O_3–Al_2O_3 diagram (after Franz & Wirth 2000); **(b)** Cr#–Mg# diagram (after Arai 1994; Kamenetsky et al. 2001); **(c)** TiO_2–Al_2O_3 diagram (after Kepezhinskas et al. 1993; Kamenetsky et al. 2001); **(d)** MnO–Cr# diagram (after Khedr & Arai 2016).

between Mg and Fe^{2+} (Fig. 6a) is observed, reflecting coupled Fe–Mg substitution during spinel crystallization. In contrast, Cr exhibits only weak correlation with Mn (Fig. 6b), and similarly weak relationships are observed between Mn and Mg (Fig. 6c) and between Mn and Fe^{2+} (Fig. 6d). These patterns indicate that Mn behaves largely independently of major Fe–Mg exchange processes.

Orthopyroxene compositions (Table 3, Supplementary Table S2) are characterized by high Mg# values (90.04–94.36), with Cr_2O_3 contents ranging from 0.19 to 0.76 wt.% and very low TiO_2 contents (<0.03 wt.%). Orthopyroxenes define systematic trends in both Mg#–Al_2O_3 and Cr_2O_3–Al_2O_3 space (Fig. 7a, b). Mg# values show a slight decrease with increasing Al_2O_3, and most analyses cluster at low Al_2O_3 (< ~2 wt.%) and high Mg# (>90). In the Cr_2O_3–Al_2O_3 diagram, orthopyroxenes display a weak negative correlation, with increasing Cr_2O_3 corresponding to decreasing Al_2O_3. Most data plot within or close to the forearc peridotite (FAP) field, with partial overlap into the abyssal peridotite (ABP) field.

Olivine compositions (Table 4, Supplementary Table S3) show Fo values of 90.52–92.63 and NiO contents of 0.19–0.54 wt.%. Olivine compositions define systematic relationships in both NiO–Fo and MnO–Fo space (Fig. 8a, b). NiO contents show a weak positive correlation with Fo, with most analyses clustering at Fo values above 90 and NiO between ~0.3 and 0.5 wt.%. In contrast, MnO contents exhibit a slight decrease with increasing Fo. These compositions fall within the range of mantle-derived peridotitic olivine and define trends consistent with increasing compositional depletion.

Calculated melt compositions derived from Cr-spinel chemistry (Fig. 9a–c) define systematic relationships between spinel and melt compositions. Al_2O_3(melt) values increase with increasing Al_2O_3(spinel) (Fig. 9a), while TiO_2(melt) shows a positive relationship with TiO_2(spinel) (Fig. 9b). In addition, FeO/MgO(melt) ratios define a coherent distribution relative to Al_2O_3(melt) (Fig. 9c). These relationships demonstrate consistent chemical linkage between spinel compositions and their calculated parental melts.

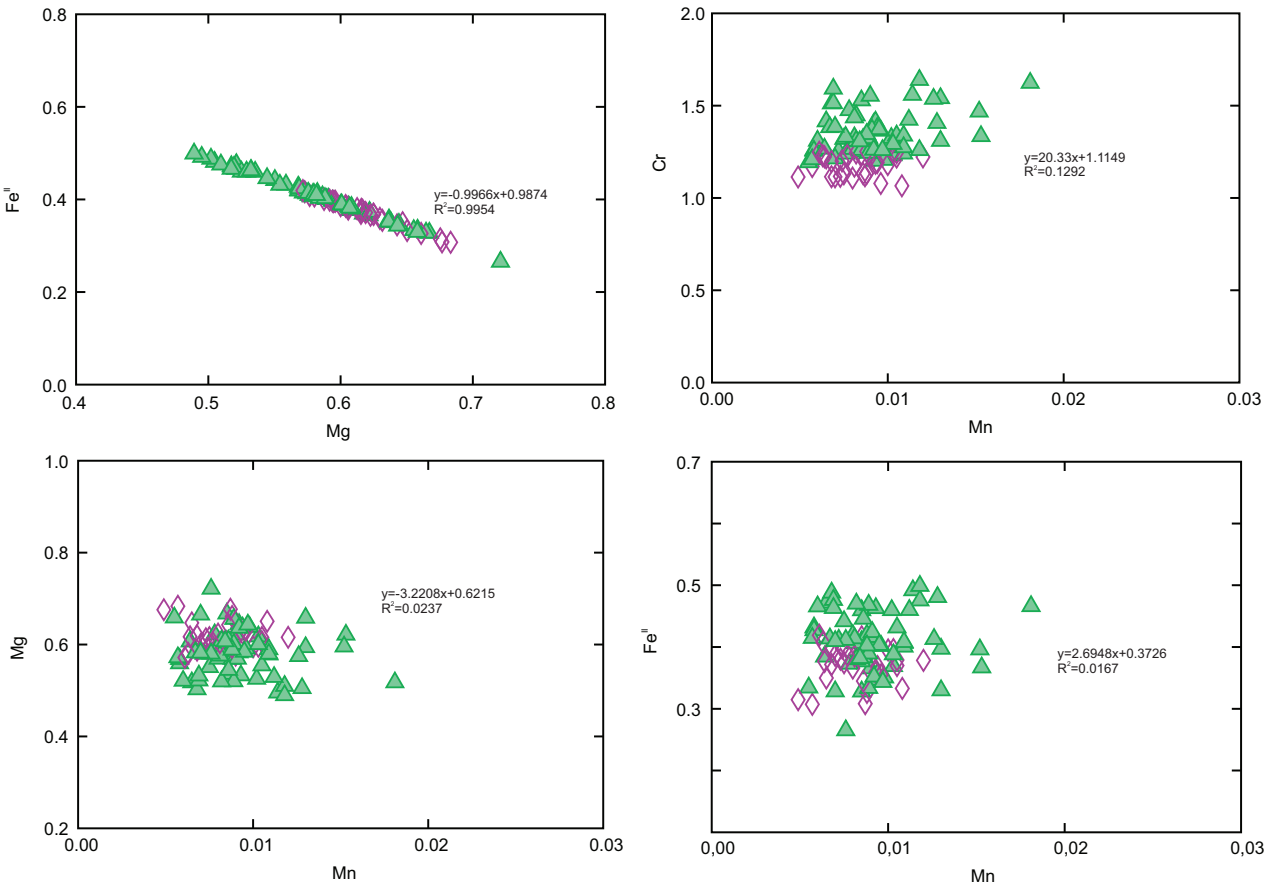

Fig. 6. Binary diagrams illustrating trace-element and divalent cation relationships in Cr-spinels from the Kağızman chromitites: **(a)** Mg versus Fe^{2+} diagram showing a strong negative correlation, reflecting coupled Fe–Mg substitution during spinel crystallization from evolving magmatic melts; **(b)** Mn versus Cr diagram displaying weak correlation, indicating limited coupling between Mn incorporation and Cr enrichment during chromitite crystallization; **(c)** Mn versus Mg diagram showing scattered distributions, suggesting that Mn behaved largely independently of major Fe–Mg exchange processes; **(d)** Mn versus Fe^{2+} diagram further supporting limited post-magmatic redistribution of Mn. Overall systematics indicate dominance of primary magmatic controls and minimal influence of secondary alteration.

Table 3: Representative electron microprobe analyses, structural formulae, and compositional parameters of orthopyroxenes from the Kağızman ophiolite chromitites. Structural formulae were calculated on the basis of 6 oxygens. Abbreviations: Wo=wollastonite component, En=enstatite component, Fs=ferrosilite component. Mg# is calculated as $Mg/(Mg+Fe^{2+})$. Sample locations and geological context are provided in Table 1.

Sample ID	ST 4X_10	ST 4X_14	ST 4X_21	LB 4_4	LB 4_6	LB 4_8
SiO_2	58.16	56.03	56.36	56.38	57.19	57.83
TiO_2	0.02	0.02	0.01	0.02	0.02	0.01
Al_2O_3	1.90	0.50	1.17	1.05	1.03	0.49
Cr_2O_3	0.54	0.53	0.57	0.34	0.36	0.19
Fe_2O_3	0.00	2.23	1.12	2.57	0.65	0.48
FeO	5.82	6.05	5.15	3.75	4.95	4.83
MnO	0.12	0.13	0.18	0.11	0.13	0.12
MgO	32.41	33.51	34.14	35.04	34.97	35.62
CaO	0.68	0.79	0.88	0.82	0.73	0.51
Na_2O	0.20	0.01	0.02	0.01	0.01	0.01
K_2O	0.00	0.01	0.00	0.00	0.00	0.00
Total	99.86	99.80	99.59	100.10	100.06	100.12
Si	1.999	1.963	1.959	1.952	1.968	1.983
Al-1	0.001	0.020	0.041	0.043	0.032	0.017
Al-2	0.076	0.000	0.007	0.000	0.010	0.003
Fe^{3+}	0.000	0.058	0.029	0.066	0.017	0.012
Cr	0.015	0.015	0.016	0.009	0.010	0.005
Ti	0.001	0.001	0.000	0.001	0.001	0.000
Fe^{2+}	0.169	0.176	0.149	0.108	0.142	0.138
Mn	0.003	0.004	0.005	0.003	0.004	0.004
Mg	1.660	1.750	1.769	1.808	1.794	1.821
Ca	0.025	0.030	0.033	0.030	0.027	0.019
Na	0.014	0.001	0.001	0.001	0.001	0.001
K	0.000	0.000	0.000	0.000	0.000	0.000
Total	3.963	4.018	4.009	4.021	4.005	4.004
Wo	1.35	1.47	1.64	1.51	1.35	0.95
En	89.37	86.71	89.11	89.68	90.44	91.30
Fs	9.28	11.83	9.25	8.81	8.21	7.75
Mg#	90.76	90.85	92.22	94.36	92.66	92.93

Discussion

Supra-subduction zone setting and mantle depletion

The chromitites of the Kağızman Ophiolite are characterized by Cr-spinel compositions displaying consistently high Cr# values and low TiO_2 contents, indicating formation within a highly depleted mantle environment. In Cr_2O_3–Al_2O_3 space (Fig. 5a), the data define a well-developed mantle array consistent with progressive melt depletion, similar to trends documented in other Neo-Tethyan ophiolitic chromitites (Proenza et al. 2008; Arai & Miura 2016). The TiO_2–Al_2O_3 systematics (Fig. 5b) show uniformly low TiO_2 contents across the dataset, consistent with derivation from low-Ti melts typical of supra-subduction zone (SSZ) settings. Most analyses plot within or close to the low-Ti arc and SSZ peridotite fields, indicating melt generation under hydrous conditions. Such melts are commonly associated with boninitic to arc-tholeiitic compositions formed during flux melting of previously depleted harzburgitic mantle (Dick & Bullen 1984; Arai 1994; Kamenetsky et al. 2001). MnO–Cr# systematics (Fig. 5c) support preservation of primary composition. However, the overall distribution indicates that primary magmatic compositions are largely preserved. The Cr#–Mg# relationship (Fig. 5d) further constrains the tectonic setting, with the majority of the data plotting within the forearc peridotite and boninite fields. This distribution is consistent with high degrees of melt depletion and interaction with high-Mg melts in a supra-subduction zone environment. The observed spread in Cr# and Mg#

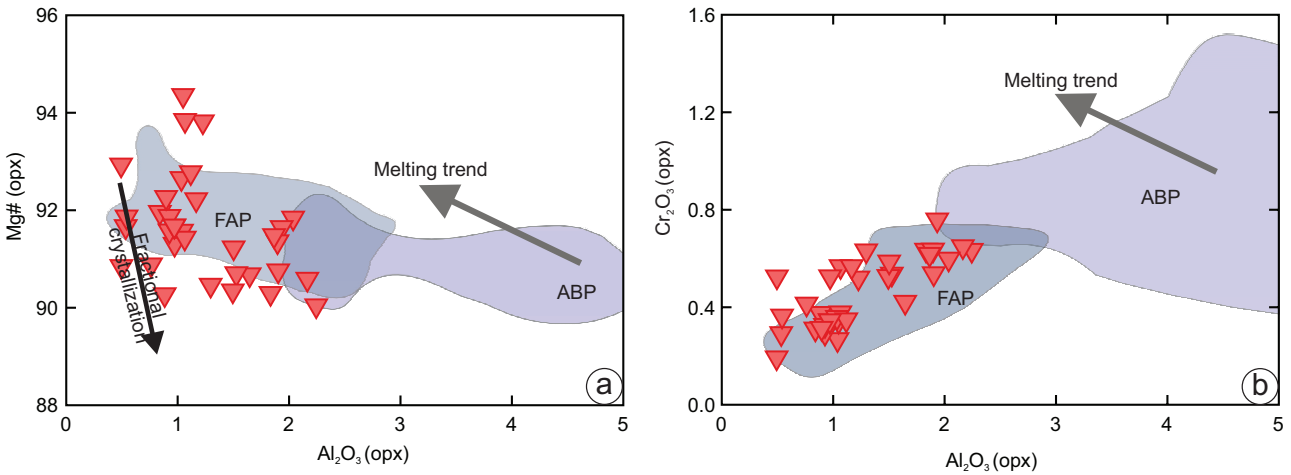

Fig. 7. Compositional variation of orthopyroxene from the Kağızman peridotites: **(a)** Mg# versus Al_2O_3 diagram showing a slight decrease in Mg# with increasing Al_2O_3. Most analyses plot within the forearc peridotite (FAP) field, with minor overlap into the abyssal peridotite (ABP) field; **(b)** Cr_2O_3 versus Al_2O_3 diagram showing a weak negative correlation, where increasing Cr_2O_3 corresponds to decreasing Al_2O_3. The data define trends consistent with progressive melt depletion. Reference fields and melting trends are after Dick & Bullen (1984) and Arai (1994).

values indicates that the system was not chemically homogeneous and likely reflects interaction with compositionally variable melts rather than crystallization from a single melt batch.

The relationship between olivine Fo content and spinel Cr# (Fig. 10) provides an integrated constraint on mantle processes by linking silicate and oxide mineral chemistry. The data define a positive correlation between Fo and Cr#, consistent with progressive melt extraction and melt–rock interaction (Dick & Bullen 1984; Arai 1994). Most samples follow melting trajectories toward higher Cr# and Fo values and plot predominantly within the field of supra-subduction zone peridotites, although limited overlap with abyssal peridotite fields is observed. This co-variation indicates a coupled petrogenetic evolution of olivine and spinel, reflecting equilibrium during progressive depletion rather than independent crystallization histories.

Orthopyroxene compositions, characterized by low Al_2O_3 and high Mg#, support high degrees of mantle depletion and are consistent with olivine–spinel systematics. However, unlike Cr-spinel, olivine and orthopyroxene compositions are not uniquely diagnostic of tectonic setting and therefore provide supporting rather than primary constraints. Overall, the combined mineral chemical data indicate that chromitite formation in the Kağızman Ophiolite occurred within a depleted mantle wedge environment, where melt–rock interaction and variable melt flux played a key role in controlling compositional variability.

Table 4: Representative electron microprobe analyses, structural formulae, and compositional parameters of olivines from the Kağızman ophiolite chromitites. Structural formulae were calculated on the basis of 4 oxygens. Abbreviations: Fo = forsterite component and Fa = fayalite component.

Sample ID	ST 4X_2	ST 4X_5	ST 4X_6	LB 4_4	LB 4_6	LB 4_14
SiO_2	41.11	42.06	42.26	42.02	42.86	39.97
TiO_2	0.02	0.02	0.01	0.02	0.02	0.01
Al_2O_3	0.03	0.02	0.03	0.02	0.02	0.01
Cr_2O_3	0.09	0.09	0.09	0.08	0.08	0.02
FeO	7.76	8.13	8.47	7.05	7.84	9.21
MnO	0.11	0.13	0.15	0.09	0.04	0.11
MgO	50.57	49.30	48.58	50.35	48.70	49.96
CaO	0.02	0.04	0.02	0.03	0.03	0.02
NiO	0.53	0.48	0.46	0.46	0.44	0.40
Total	100.23	100.25	100.06	100.13	100.04	99.71
Si	1.000	1.021	1.029	1.017	1.038	0.985
Ti	0.000	0.000	0.000	0.000	0.000	0.000
Al	0.001	0.000	0.001	0.001	0.001	0.000
Cr	0.002	0.002	0.002	0.002	0.002	0.000
Fe^{2+}	0.158	0.165	0.172	0.143	0.159	0.190
Mn	0.002	0.003	0.003	0.002	0.001	0.002
Mg	1.834	1.785	1.763	1.817	1.759	1.836
Ni	0.000	0.001	0.000	0.001	0.001	0.000
Ca	0.014	0.012	0.012	0.012	0.011	0.010
Total	3.012	2.990	2.982	2.993	2.971	3.025
Fo	91.97	91.41	90.95	92.63	91.68	90.52
Fa	7.92	8.46	8.89	7.28	8.27	9.36
Tp	0.11	0.14	0.16	0.09	0.04	0.12
Mg#	92.07	91.53	91.09	92.72	91.72	90.63

Melt–rock interaction and primary magmatic signatures

Petrographic observations provide important constraints on the processes responsible for chromitite formation in the Kağızman Ophiolite. Chromitites occur as massive to disseminated bodies hosted by dunite envelopes within serpentinized harzburgite, consistent with focused melt flow and reactive channel formation in the upper mantle. The preservation of sharp Cr-spinel grain boundaries and the occurrence of primary silicate inclusions enclosed within spinel indicate limited post-magmatic re-equilibration.

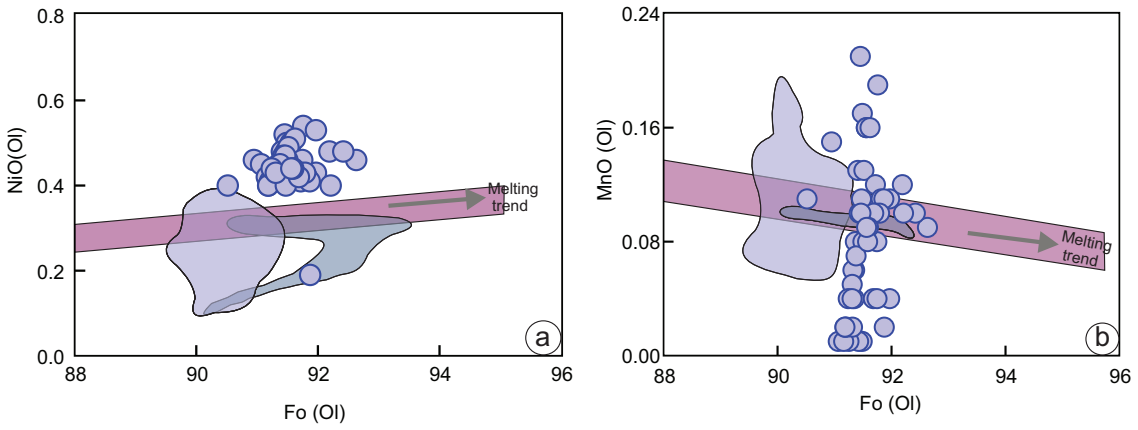

Fig. 8. Compositional relationships between olivine Fo content and minor element concentrations: **(a)** NiO versus Fo diagram showing a weak positive correlation, consistent with mantle olivine compositions and progressive melt depletion trends; **(b)** MnO versus Fo diagram showing a slight negative correlation, reflecting typical mantle fractionation behavior. Reference fields and trends for mantle olivine are shown for comparison. Most analyses cluster at high Fo values (>90), indicating a highly depleted mantle source.

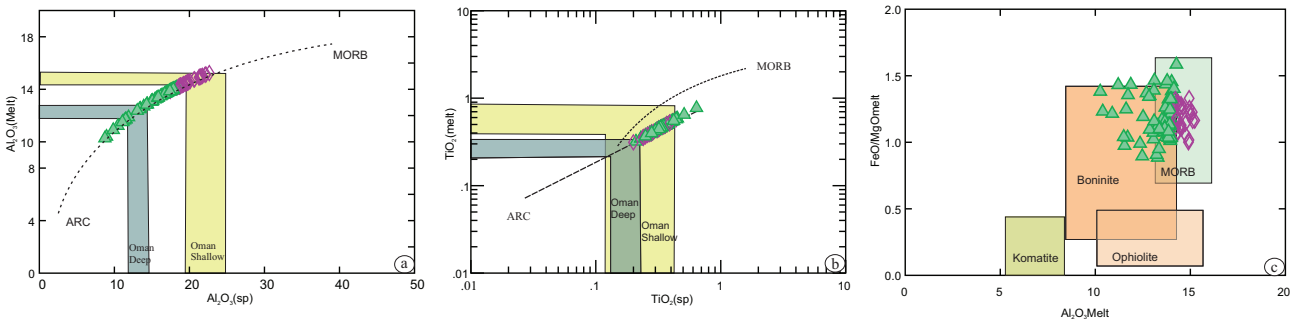

Fig. 9. Calculated parental melt compositions in equilibrium with chromian spinels from the Kağızman chromitites. **(a)** Al_2O_3(spinel)–Al_2O_3(melt) and **(b)** TiO_2(spinel)–TiO_2(melt) diagrams. MORB and arc trends are after Rollinson (2008), whereas Oman Deep and Oman Shallow boninite fields are from Ishikawa et al. (2002). **(c)** FeO/MgO(melt) versus Al_2O_3(melt) diagram showing the affinity of the calculated melts with boninitic compositions; reference fields are modified after Barnes & Roeder (2001) and Merlini et al. (2011).

Cr-spinel compositions plotting along the Cr–Al join with very low Fe^{3+} proportions are consistent with low degrees of oxidation and preservation of primary magmatic chemistry (Arai 1992; Proenza et al. 1999) (Fig. 4a). This interpretation is further supported by the inverse Cr#–Mg# relationship (Fig. 5d), which is characteristic of spinels formed during melt extraction and melt–peridotite interaction in supra-subduction zone settings (Dick & Bullen 1984; Arai 1994).

Trace-element and divalent cation systematics of Cr-spinels further support the preservation of primary magmatic signatures (Fig. 6a–d). A strong negative correlation between Mg and Fe^{2+} (Fig. 6a) reflects coupled Fe–Mg substitution during spinel crystallization and indicates equilibrium partitioning between melt and mineral phases (Irvine 1967; Kamenetsky et al. 2001). In contrast, Cr shows only weak correlation with Mn (Fig. 6b), and similarly weak relationships are observed between Mn and Mg (Fig. 6c) and between Mn and Fe^{2+} (Fig. 6d). These weak correlations suggest that Mn was not significantly involved in Fe–Mg exchange processes and was primarily controlled by crystal–melt partitioning rather than post-magmatic redistribution (Rollinson 2008).

These mineral-chemical relationships, together with petrographic observations, indicate that the primary geochemical signatures preserved in Cr-spinel reflect melt–rock interaction processes in a depleted mantle environment (Arai 1994; Kamenetsky et al. 2001). The compositional trends observed in Cr_2O_3–Al_2O_3 space (Fig. 5a) further support progressive melt depletion and interaction between migrating melts and refractory mantle peridotite (Dick & Bullen 1984). Importantly, the wide range of Cr# values indicates that chromitite formation cannot be attributed to a single homogeneous melt. Instead, part of the compositional variability likely reflects interaction with compositionally variable melts, dominated by highly depleted supra-subduction zone melts and, to a lesser extent, melts with more MORB-like characteristics (Pearce et al. 2000; Rollinson & Adetunji 2013). However, the overall coherence of the geochemical trends and the consistently low TiO_2 contents indicate that melt–rock interaction processes operated predominantly within a depleted mantle system.

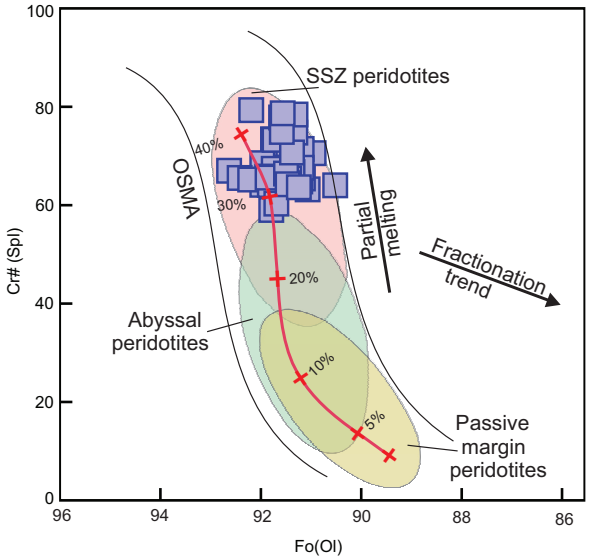

Fig. 10. Relationship between olivine Fo content and spinel Cr# for samples from the Kağızman Ophiolite. The data define a positive correlation reflecting progressive melt depletion and melt–rock interaction within a supra-subduction zone mantle environment. The evolutionary trend is consistent with increasing degrees of partial melting, with most samples plotting within the supra-subduction zone (SSZ) peridotite field and showing limited overlap with abyssal peridotite compositions (after Dick & Bullen 1984; Arai 1994).

Constraints on parental melt composition in a supra-subduction zone setting

Spinel–melt compositional systematics provide robust constraints on the nature and evolution of parental melts responsible for chromitite formation in the Kağızman Ophiolite. Calculated melt compositions derived from Cr-spinel chemistry plot predominantly within, or close to, the boninite and arc-related fields on Al_2O_3(melt)–Al_2O_3(spinel) and TiO_2(melt)–TiO_2(spinel) diagrams (Fig. 9a, b). These systematics indicate derivation from high-Mg, low-Ti melts characteristic of supra-subduction zone (SSZ) forearc environments

(Parkinson & Pearce 1998; Kamenetsky et al. 2001; Tamura & Arai 2006).

The low TiO_2 contents inferred for the parental melts (Fig. 9b) indicate melting under conditions of prior mantle depletion and the influence of slab-derived fluids. Such low-Ti melt signatures are widely associated with boninitic magmatism generated during subduction initiation, where hydrous flux melting affects refractory mantle sources (Arai 1994; Pearce et al. 2000). The Kağızman data show close similarity to calculated melt compositions reported from SSZ chromitites in the Oman and western Neo-Tethyan ophiolites.

Further constraints are provided by the FeO/MgO versus Al_2O_3(melt) relationship (Fig. 9c), where the inferred melts plot mainly within the boninite–ophiolite fields and are largely distinct from typical MORB melt trends (Rollinson 2008; Dilek & Furnes 2011). This relationship reflects interaction with highly magnesian melts produced by high degrees of partial melting and efficient melt–rock reaction, rather than simple melt extraction from fertile mantle sources.

Although the calculated melt compositions cluster within SSZ-related fields, minor dispersion of the data indicates limited compositional variability. This variability likely reflects differences in melt evolution, melt/rock interaction intensity, and small-scale heterogeneity within the mantle source region. However, the overall coherence of the data and the consistently low TiO_2 contents indicate that the parental melts were predominantly derived from a depleted mantle source influenced by subduction-related processes.

Taken together, the spinel–melt relationships indicate that chromitite formation in the Kağızman Ophiolite was largely controlled by hydrous melting of a refractory mantle source during subduction initiation. Episodic infiltration of compositionally evolving melts likely resulted in localized chromitite saturation within dunite channels, consistent with the petrographic and mineral-chemical observations.

Implications for chromitite genesis and forearc mantle evolution along the İzmir–Ankara–Erzincan Suture Zone

Recent studies from the İzmir–Ankara–Erzincan Suture Zone (IAESZ) indicate that podiform chromitites are closely associated with supra-subduction zone (SSZ) processes operating during subduction initiation and early forearc evolution (Arai 1994; Pearce et al. 2000; Dilek & Furnes 2011). Within this framework, the Kağızman chromitites provide important constraints on chromitite-forming processes in the eastern segment of the IAESZ and allow comparison with chromitite-bearing ophiolites across the Neo-Tethyan domain.

As illustrated in Fig. 11a, chromitites from different segments of the IAESZ and adjacent regions define comparable compositional trends, characterized by consistently high Cr# values, moderate to high Mg#, and low TiO_2 contents. These features are widely interpreted as reflecting formation from melts interacting with a depleted mantle source and are characteristic of SSZ-related chromitites. The Kağızman dataset follows these regional trends, supporting its affinity with a mantle system developed along the northern margin of the Neo-Tethys.

However, the relatively wide compositional range observed in the Kağızman samples, particularly in Cr#, indicates that chromitite formation cannot be explained by a single, uniform melt evolution pathway. Instead, this variability reflects differences in melt flux, melt/rock ratios, and the temporal evolution of melt infiltration processes within the mantle wedge.

The conceptual model shown in Fig. 11b illustrates the geodynamic framework for chromitite formation during subduction initiation and forearc development. In the back-arc or oceanic domain, MORB-type mantle is associated with relatively low-Cr# chromitites formed under lower degrees of depletion. In contrast, within the forearc mantle wedge, slab-derived fluids promote hydrous partial melting of a refractory mantle source, generating boninitic, high-Mg melts. These melts are focused into dunite channels, where melt–rock interaction leads to orthopyroxene dissolution and progressive enrichment of Cr relative to Al, ultimately triggering chromitite saturation and the formation of high-Cr# chromitites. The juxtaposition of different mantle domains during ophiolite emplacement further contributes to the observed compositional variability. This framework explains the coexistence of chromitites with variable Cr# values and is consistent with the mineral-chemical trends observed in the Kağızman dataset (Figs. 5 and 9).

The combined mineral-chemical data further support this interpretation. The positive correlation between olivine Fo and spinel Cr# (Fig. 10) indicates that both minerals record a common history of progressive melt extraction. Orthopyroxene compositions, characterized by low Al_2O_3 and high Mg#, are consistent with high degrees of depletion and support the same melting regime. Although olivine and orthopyroxene alone are not uniquely diagnostic of tectonic setting, their coupled behavior with spinel strengthens the interpretation that all mineral phases record a coherent petrogenetic evolution.

In addition to this dominant process, part of the observed compositional variability may reflect differences in melt evolution and melt–rock interaction conditions within the mantle wedge. The partial overlap between compositional fields in different IAESZ segments (Fig. 11a) suggests that some compositions approach those typical of less depleted systems; however, this does not require contributions from distinct mantle domains.

Taken together, the regional comparison and process-based model indicate that chromitite formation in the Kağızman Ophiolite was largely controlled by hydrous melt–rock interaction in a variably depleted mantle during subduction initiation. The integrated behavior of spinel, olivine, and orthopyroxene supports a coherent melting history, while local compositional variability reflects the complexity of melt evolution and mantle heterogeneity within the forearc environment.

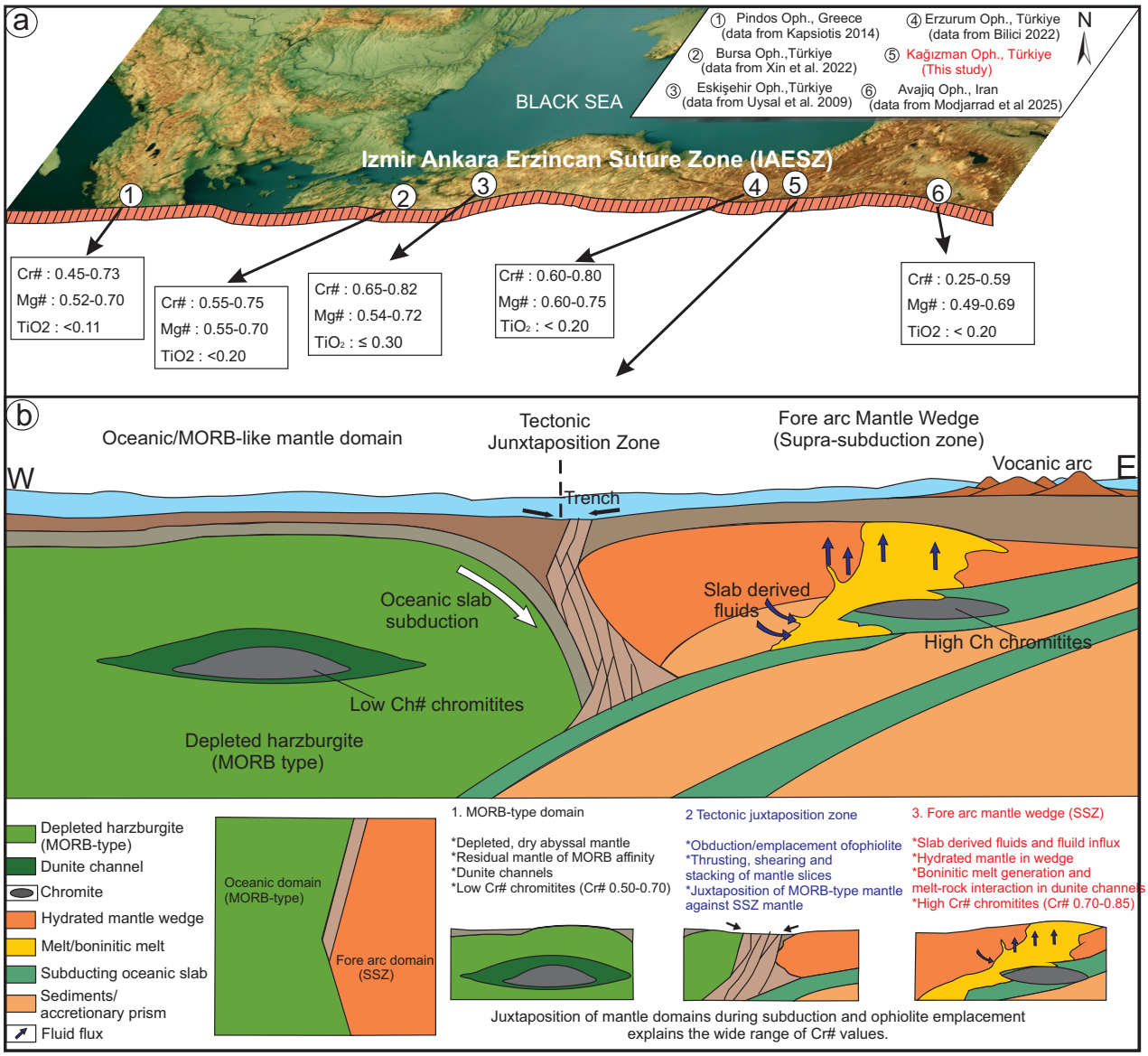

Fig. 11. (a) Comparison of Cr-spinel compositions from the Kağızman Ophiolite and other chromitite-bearing ophiolites along the İzmir–Ankara–Erzincan Suture Zone (IAESZ), showing similar trends characterized by high Cr#, moderate to high Mg#, and low TiO_2 contents. **(b)** Conceptual model for chromitite formation during subduction initiation, illustrating hydrous melting of a depleted mantle wedge, melt focusing in dunite channels, and chromitite crystallization through melt–rock interaction.

Conclusions

- Podiform chromitites from the Kağızman Ophiolite record formation within a variably depleted mantle environment associated with supra-subduction zone (SSZ) processes during subduction initiation along the eastern segment of the İzmir–Ankara–Erzincan Suture Zone.
- Cr-spinel compositions, characterized by consistently high Cr# values and low TiO_2 contents, provide the primary constraints on tectonic setting. In contrast, olivine and orthopyroxene compositions indicate high degrees of mantle depletion but are not uniquely diagnostic of SSZ environments, serving instead as supporting constraints.
- Systematic relationships between olivine Fo and spinel Cr# demonstrate a coupled petrogenetic evolution and indicate that silicate and oxide minerals record a common history of progressive melt extraction and melt–rock interaction.
- Petrographic observations and mineral-chemical systematics indicate that chromitite formation was controlled by focused melt flow and reactive melt–rock interaction within dunite channels in a depleted mantle wedge.
- The observed compositional variability, particularly in Cr#, indicates that chromitite formation cannot be explained by a single homogeneous melt, but rather reflects interaction with compositionally variable melts and evolving melt flux conditions.

- Regional comparisons across the İzmir–Ankara–Erzincan Suture Zone demonstrate that similar SSZ-related chromitite-forming processes operated along the Neo-Tethyan margin, although local variability reflects differences in melt flux, melt/rock ratios, and mantle heterogeneity.
- Overall, the Kağızman Ophiolite provides a well-constrained case study of chromitite formation during subduction initiation, highlighting the importance of integrating Cr-spinel systematics with silicate mineral chemistry and petrographic evidence to resolve mantle processes in forearc settings.

Acknowledgements: This work forms part of the MSc thesis of Levent Aslan and was supported by the Scientific Research Projects Coordination Unit of Van Yüzüncü Yıl University (Project No. FYL-2020-8817). The authors thank the university for providing financial support for this research.

References

Arai S. 1992: Chemistry of chromian spinel in volcanic rocks as a potential guide to magma chemistry. *Mineralogical Magazine* 56, 173–184. https://doi.org/10.1180/minmag.1992.056.383.04

Arai S. 1994: Characterization of spinel peridotites by olivine–spinel compositional relationships: Review and interpretation. *Chemical Geology* 113, 191–204. https://doi.org/10.1016/0009-2541(94)90066-3

Arai S. 2013: Conversion of low-pressure chromitites to ultrahigh-pressure chromitites by deep recycling: a good inference. *Earth and Planetary Science Letters* 379, 81–87. https://doi.org/10.1016/j.epsl.2013.08.006

Arai S. & Miura M. 2016: Formation and modification of chromitites in the mantle. *Lithos* 264, 277–295. https://doi.org/10.1016/j.lithos.2016.08.039

Aslan E., Parlak O., Zhang C., Wang J., Lian D., Xu Y., Chen G., Robertson A., Yang J., Xu X. & Hong J. 2025: Geochemistry of mantle peridotites and chromitites from Upper Cretaceous ophiolite in NW Türkiye: Insights into abyssal to forearc mantle setting. *Lithos* 514–515, 108208. https://doi.org/10.1016/j.lithos.2025.108208

Barnes SJ. & Roeder PL. 2001: The Range of Spinel Compositions in Terrestrial Mafic and Ultramafic Rocks. *Journal of Petrology* 42, 2279–2302. https://doi.org/10.1093/petrology/42.12.2279

Bilici Ö. 2022: Reactive harzburgite and ultimate dunite formation as a result of boninite-like melt interaction: Petrological evidence from the Kırdag ophiolite (Erzurum, NE Turkey). *Journal of African Earth Science* 193, 104601. https://doi.org/10.1016/j.jafrearsci.2022.104601

Bilici Ö. 2025: Highly siderophile elements and mineral chemistry of chromitites from the Kırdağ ophiolite (NE Turkey): Constraints on genesis and subduction initiation. *Journal of African Earth Sciences* 230, 105726. https://doi.org/10.1016/j.jafrearsci.2025.105726

Dick H.J.B. & Bullen T. 1984: Chromian spinel as a petrogenetic indicator in abyssa and Alpine-type peridotites and spatially associated lavas. *Contribution to Mineralogy and Petrology* 86, 54–76.

Dilek Y. & Furnes H. 2011: Ophiolite genesis and global tectonics: Geochemical and tectonic fingerprinting of ancient oceanic lithosphere. *Geological Society of America Bulletin* 123, 387–411. https://doi.org/10.1130/B30446.1

Farré-de-Pablo J., Proenza J.A., González-Jiménez J.M., Aiglsperger T., Garcia-Casco A., Escuder-Viruete J., Colás V. & Longo F. 2020: Ophiolite hosted chromitite formed by supra-subduction zone peridotite–plume interaction. *Geoscience Frontiers* 11, 2083–2102. https://doi.org/10.1016/j.gsf.2020.05.005

Fornasaro S., Comodi P., Crispini L., Zappatore S., Zucchini A. & Marescotti P. 2023: Trace and ultratrace elements in spinel subgroup minerals of ultramafic rocks from the Voltri Massif (NW Italy): the influence of microstructure and texture. *European Journal of Mineralogy* 35, 1091–1109. https://doi.org/10.5194/ejm-35-1091-2023

Franz L. & Wirth R. 2000: Spinel inclusions in olivine of peridotite xenoliths from TUBAF seamount (Bismarck Archipelago/Papua New Guinea): evidence for the thermal and tectonic evolution of the oceanic lithosphere. *Contributions to Mineralogy and Petrology* 140, 283–295. https://doi.org/10.1007/s004100000188

Herzberg C., Cabral R.A., Jackson M. G., Vidito C., Day J. M. D. & Hauri E. H. 2014: Phantom Archean crust in Mangaia hotspot lavas and the meaning of heterogeneous mantle. *Earth and Planetary Science Letters* 396, 97–106. https://doi.org/10.1016/j.epsl.2014.03.065

Irvine T.N. 1967: Chromian spinel as a petrogenetic indicator. Part 2. Petrologic applications. *Canadian Journal of Earth Sciences* 4, 71–103.

Ishikawa T., Nagaishi K. & Umino S. 2002: Boninitic volcanism in the Oman ophiolite: implications for thermal condition during transition from spreading ridge to arc. *Geology* 30, 899–902. https://doi.org/10.1130/0091-7613(2002)030<0899:BVITOO>2.0.CO;2

Kamenetsky V.S., Crawford A.J. & Meffre S. 2001: Factors controlling chemistry of magmatic spinel: an empirical study of associated olivine, Cr-spinel and melt inclusions from primitive rocks. *Journal of Petrology* 42, 655–671. https://doi.org/10.1093/petrology/42.4.655

Kapsiotis A. 2013: Genesis of chromitites from Korydallos, Pindos Ophiolite Complex, Greece, based on spinel chemistry and PGE-mineralogy. *Journal of Geosciences* 58, 49–69. https://doi.org/10.3190/jgeosci.133

Kapsiotis A. 2014: Composition and alteration of Cr-spinels from Milia and Pefki serpentinized mantle peridotites (Pindos Ophiolite Complex, Greece). *Geologıca Carpathıca* 65, 83–95. https://doi.org/10.2478/geoca-2013-0006

Kepezhinskas P.K., Taylor R.N. & Tanaka H. 1993: Geochemistry of plutonic spinels from the North Kamchatka Arc: comparisons with spinels from other tectonic settings. *Mineralogical Magazine* 57, 575–589. https://doi.org/10.1180/minmag.1993.057.389.02

Khedr M.Z. & Arai S. 2016: Chemical variations of mineral inclusions in Neoproterozoic high-Cr chromitites from Egypt: Evidence of fluids during chromitite genesis. *Lithos* 240–243, 309–326. https://doi.org/10.1016/j.lithos.2015.11.029

Knipper A.L., Ricon L.-E. & Dercourt J. 1986: Ophiolites as indicators of the Alpine history of the Tethyan ocean. *Tectonophysics* 123, 213–240. https://doi.org/10.1016/0040-1951(86)90198-8

Liu X., Su B.X., Gopon P., Xiao Y. & Uysal I. 2023: Post-magmatic hydrothermal activities in the Bursa ophiolite (NW Turkey): Implications for unusual minerals recovered from ophiolites. *Lithos* 436–437, 106957. https://doi.org/10.1016/j.lithos.2022.106957

Merlini A., Grieco G., Ottolini L. & Diella V. 2011: Probe and SIMS investigation of clinopyroxene inclusions in chromites from the Troodos chromitites (Cyprus): implications for dunite–chromitite genesis. *Ore Geology Reviews* 41, 22–34. https://doi.org/10.1016/j.oregeorev.2011.06.002

Miura M., Arai S., Ahmed A.H., Mizukami T., Okuno M. & Yamamoto S. 2012: Podiform chromitite classification revisited: A comparison of discordant and concordant chromitite pods from Wadi Hilti, northern Oman ophiolite. *Journal of Asian Earth Sciences* 59, 52–61. https://doi.org/10.1016/j.jseaes.2012.05.008

Modjarrad M., Uysal I., Moghadam H.S., Demir Y. & Müller D. 2025: Geochemical insights and petrogenetic processes of ophiolitic fragments from the Avajiq and Silvana: implications for Neo-Tethyan Evolution in Northwest Iran. *International Geology Review* 67, 1437–1465. https://doi.org/10.1080/00206814.2025.2453979

Moghadam H.S., Li Q.L., Li X.H., Stern R.J., Levresse G., Santos J.F., Martinez M.L., Ducea M.N., Ghorbani G. & Hassannezhad A. 2020: Neotethyan Subduction Ignited the Iran Arc and Back-arc Differently. *Journal of Geophysical Research: Solid Earth* 125, 2019JB018460. https://doi.org/10.1029/2019JB018460

Okay A.I. & Tüysüz O. 1999: Tethyan sutures of northern Turkey. *Geological Society, London, Special Publications* 156, 475–515. https://doi.org/10.1144/GSL.SP.1999.156.01.22

Okay A.I. & Şengör A.M.C. 1992: Evidence for HP/LT metamorphism in the Pontides, Turkey: Implications for Tethyan subduction history. *Tectonophysics* 201, 119–147.

Parkinson I.J. & Pearce J.A. 1998: Peridotites from the Izu–Bonin–Mariana forearc (ODP Leg 125): Evidence for mantle melting and melt-mantle interaction in a supra-subduction zone setting. *Journal of Petrology* 39, 1577–1618. https://doi.org/10.1093/petroj/39.9.1577

Pearce J. 2014: Geochemical fingerprinting of the Earth's Oldest Rocks. *Geology* 42, 175–176. https://doi.org/10.1130/focus022014.1

Pearce J.A., Lippard S.J. & Roberts S. 1984: Characteristics and tectonic significance of supra-subduction zone ophiolites. *Geological Society, London, Special Publications* 16, 77–94. https://doi.org/10.1144/GSL.SP.1984.016.01.06

Pearce J.A., Barker P.F., Edwards S.J., Parkinson I.J. & Leat P.T. 2000: Geochemistry and tectonic significance of peridotites from the south sandwich arc–basin system, South Atlantic. *Contributions to Mineralogy and Petrology* 139, 36–53.

Proenza J.A. Gervilla F. Melgarejo J.C. & Bodinier J.L. 1999: Al- and Cr-rich chromitites from the Mayari-Baracoa ophiolitic belt (eastern Cuba); consequence of interaction between volatile-rich melts and peridotites in suprasubduction mantle. *Economic Geology* 94, 547–566. https://doi.org/10.2113/gsecongeo.94.4.547

Proenza J.A., Zaccarini F., Escayola M., Cabana C., Schalamuk A. & Garuti G. 2008: Composition and textures of chromite and platinum-group minerals in chromitites of the western ophiolitic belt from Pampean Ranges of Córdoba, Argentina. *Ore Geology Rewiev* 33, 32–48. https://doi.org/10.1016/j.oregeorev.2006.05.009

Robertson A., Parlak O., Ustaömer T., Taşlı K., İnan N., Dumitrica P. & Karaoğlan F. 2014: Subduction, ophiolite genesis and collision history of Tethys adjacent to the Eurasian continental margin: new evidence from the Eastern Pontides, Turkey. *Geodinamica Acta* 26, 230–293. https://doi.org/10.1080/09853111.2013.877240

Rolland Y. 2017: Caucasus collisional history: Review of data from East Anatolia to West Iran. *Gondwana Research* 49, 130–146. https://doi.org/10.1016/j.gr.2017.05.005

Rollinson H. 2008: The geochemistry of mantle chromitites from the northern part of the Oman ophiolite: inferred parental melt compositions. *Contribution to Mineralogy and Petrology* 156, 273–288. https://doi.org/10.1007/s00410-008-0284-2

Rollinson H.R. & Adetunji J. 2013: Mantle Podiform chromitites do not form beneath ocean ridges: A case study from the Moho transition zone of the Oman ophiolite. *Lithos* 177, 314–327. https://doi.org/10.1016/j.lithos.2013.07.004

Şaroğlu F., Emre Ö. & Kuşçu İ. 1992: *Active fault map of Turkey*. General Directorate of Mineral Research and Exploration (MTA), Ankara, Turkey.

Şengör A.M.C. & Yılmaz Y. 1981: Tethyan evolution of Turkey: A plate tectonic approach. Tectonophysics 75, 181–241. https://doi.org/10.1016/0040-1951(81)90275-4

Shervais J.W. & Jean M.M. 2012: Inside the subduction factory: Modeling fluid mobile element enrichment in the mantle wedge above a subduction zone. *Geochimica et Cosmochimica Acta* 95, 270–285. https://doi.org/10.1016/j.gca.2012.07.006

Sobolev A.V., Hofmann A.W., Sobolev S.V. & Nikogosian I.K. 2005: An olivine-free mantle source of Hawaiian shield basalt. *Nature* 434, 590–597. https://doi.org/10.1038/nature03411

Stampfli G.M. & Borel G.D. 2002: A plate tectonic model for the Paleozoic and Mesozoic constrained by dynamic plate boundaries and restored synthetic oceanic isochrons. *Earth and Planetary Science Letters* 196, 17–33. https://doi.org/10.1016/S0012-821X(01)00588-X

Sümengen M. 2009: *Ağrı Sheet (J50). 1:100,000 Scale Geological Map Series of Turkey*. General Directorate of Mineral Research and Exploration (MTA), Geological Survey Department Publication No. 108, Ankara, 1–18.

Tamura A. & Arai S. 2006: Harzburgite–dunite–orthopyroxenite suite as a record of supra-subduction zone setting for the Oman ophiolite mantle. *Lithos* 90, 43–56. https://doi.org/10.1016/j.lithos.2005.12.012

Uysal İ., Zaccarını F., Sadıklar M.B., Tarkıan M., Thalhammer O.A.R. & Garutı G. 2009: The podiform chromitites in the Dagküplü and Kavak mines, Eskişehir ophiolite (NW-Turkey): Genetic implications of mineralogical and geochemical data. *Geologica Acta* 7, 351–362. https://doi.org/10.1344/105.000001442

Uysal İ., Şen A.D., Ersoy E.Y., Dilek Y., Saka S., Zakkarini F., Escayola M. & Karslı O. 2014: Geochemical make-up of oceanic peridotites from NW Turkey and the multi-stage melting history of the Tethyan upper mantle. *Mineralogy and Petrology* 108, 49–69. https://doi.org/10.1007/s00710-013-0277-3

van Hinsbergen D.J.J., Torsvik T.H., Schmid S.M., Matenco L.C., Maffione M., Vissers R.L.M., Gurer D. & Spakman W. 2020: Orogenic architecture of the Mediterranean region and kinematic reconstruction of its tectonic evolution since the Triassic. *Gondwana Research* 81, 79–229. https://doi.org/10.1016/j.gr.2019.07.009

Xin G.Y., Chu Y., Su B.X., Lin W., Cui M.M., Liu X., Uysal İ., Li J.L. & Feng Z.T. 2022: Subduction initiation in the Neo-Tethys and formation of the Bursa ophiolite in NW Turkey. *Lithos* 422–423, 106746. https://doi.org/10.1016/j.lithos.2022.106746

Xiong Q., Dai H.K., Zheng J.P., Griffin W.L., Zheng H.D., Wang L. & O'Reilly S.Y. 2022: Vertical depletion of ophiolitic mantle reflects melt focusing and interaction in sub-spreading-center asthenosphere. *Nature Communications* 13. 6956. https://doi.org/10.1038/s41467-022-34781-w

Electronic supplementary material is available online:
Supplementary Table S1 at https://geologicacarpathica.com/data/files/supplements/GC-77-4-Aslan_TableS1.docx
Supplementary Table S2 at https://geologicacarpathica.com/data/files/supplements/GC-77-4-Aslan_TableS2.docx
Supplementary Table S3 at https://geologicacarpathica.com/data/files/supplements/GC-77-4-Aslan_TableS3.docx